ACS APPLIED MATERIALS & INTERFACES

Research Article

www.acsami.org

Dual-Targeting Nanosystem for Enhancing Photodynamic Therapy Efficiency

Jiangsheng Xu, Fang Zeng,* Hao Wu, Changmin Yu, and Shuizhu Wu*

College of Materials Science and Engineering, State Key Laboratory of Luminescent Materials and Devices, South China University of Technology, Guangzhou 510640, China

Supporting Information

ABSTRACT: Photodynamic therapy (PDT) has been recognized as a valuable treatment option for localized cancers. Herein, we demonstrate a cellular and subcellular targeted strategy to facilitate PDT efficacy. The PDT system was fabricated by incorporating a cationic porphyrin derivative (MitoTPP) onto the polyethylene glycol (PEG)-functionalized and folic acid-modified nanographene oxide (NGO). For this PDT system, NGO serves as the carrier for MitoTPP as well as the quencher for MitoTPP's fluorescence and singlet oxygen ($^1O_2$) generation. Attaching a hydrophobic cation to the photosensitizer ensures its release from NGO at lower pH values as well as its mitochondria-targeting capability. Laser confocal microscope experiments demonstrate that this dual-targeted nanosystem could preferably enter the cancer cells overexpressed with folate receptor, and release its cargo MitoTPP, which subsequently accumulates in mitochondria. Upon light irradiation, the released MitoTPP molecules generate singlet oxygen and cause oxidant damage to the mitochondria. Cell viability assays suggest that the dual-targeted nanohybrids exhibit much higher cytotoxicity toward the FR-positive cells.

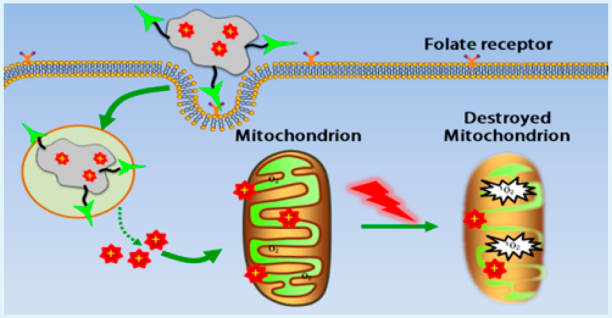

KEYWORDS: *dual-targeting, mitochondria, photodynamic therapy, drug delivery, graphene oxide*

INTRODUCTION

Photodynamic therapy (PDT), which involves the combination of light, a photosensitizer (PS), and molecular oxygen, is a promising approach in disease treatment.[1−4] It has been widely used in both oncological and nononcological applications such as tumors, dysplasias, age-related macular degeneration, and localized infection. Upon appropriate wavelength irradiation in the targeted tissues, the key cytotoxic agent, singlet oxygen ($^1O_2$), is produced and then reacts rapidly with cellular components to cause oxidative lesions and ultimately leads to apoptosis or necrosis of abnormal cells.[5−7] Compared to conventional treatment methods, PDT exhibits its own merits due to its minimal invasiveness, repeatability without cumulative toxicity, excellent functional and cosmetic results, reduced long-term morbidity, and improved quality of life of the patients.[1] Over the last several years, PDT has been employed as a valuable treatment option for solid tumors, such as superficial bladder cancer, early and obstructive lung cancer, head and neck cancers, and so on.[8,9] PDT is also used to treat precancers of the skin, and is being tested against precancers in the mouth and other places; it is being used as an adjunctive therapy following surgical resection of tumor, to reduce residual tumor burden.[10] Up to now, three generations of photosensitizers (PS) have been developed, and several photosensitizing agents, such as porfimer sodium, aminolevulinic acid (ALA), and methyl ester of ALA, are approved by the U.S. Food and Drug Administration to treat certain cancers.[11] Currently, nanomaterials represent an emerging technology in the field of PDT that can further promote the utility of classic PS, and a great number of nanoplatforms have been designed out of a variety of naturally occurring or synthetic materials and can be engineered to carry multiple theranostic agents, in a targeted manner.[8]

Generally, PS is given through intravenous injection. It travels through the bloodstream and is absorbed by both normal and cancer cells all over the body. Thus, to reduce the dose of PS administered to patients and hence minimize the harmful side-effects of PDT, rational designs should be devised to increase the efficacy of PDT through targeted delivery of PS to abnormal cells. However, delivery of PS to the tumor site is unlikely to be sufficient to elicit a maximum therapeutic response as the drug must reach the intracellular target sites. Efficient organelle-specific delivery or delivery of the drug or the drug-loaded nanosystems directly to the site of drug action is required to achieve maximum therapeutic with a minimum of off-target effects.

Mitochondria are energy factories of biological systems and play important roles in energy metabolism of various biochemical processes,[12−14] and they are also the executioners of programmed cell death (apoptosis).[15,16] Because mitochon-

Received: March 16, 2015
Accepted: April 15, 2015
Published: April 15, 2015

ACS Publications © 2015 American Chemical Society

DOI: 10.1021/acsami.5b02297
ACS Appl. Mater. Interfaces 2015, 7, 9287−9296

dria are crucial in executing apoptosis-mediated cell death and cancer cells have suppressed apoptosis, mitochondria-directed drugs designed to trigger apoptosis are likely to be promising treatment strategies for curbing cancer. To date, a number of strategies for the delivery of biologically active molecules to the mitochondria of live mammalian cells have been demonstrated;[17−20] For example, Murphy and Smith's group have designed a series of triphenylphosphonium-modified molecules with excellent mitochondria targeting capability.[13] On the other hand, Sheu et al. covalently linked trimethylammonium into their choline ester antioxidants to target mitochondria.[21] As for the PDT, some studies indicated that the photosensitizers which were modified to target the mitochondria were more effective as apoptogenic agents once irradiated.[9]

As a class of photosensitizers, porphyrin derivatives have been extensively studied due to their multiple advantages,[22−24] such as efficient production of singlet oxygen, high absorption coefficient in the long wavelength region, well-established synthetic route, etc. Recently, mitochondria-specific porphyrins have also been designed and fabricated by taking advantage of the preferential localization of lipophilic cations in mitochondria.[25] You et al. have designed and evaluated several cationic-dye-modified porphyrins for targeting mitochondria.[9,26] Wang exploited triethylammonium-modified porphyrins and compared its PDT efficiency with that of a triphenylphosphonium-modified porphyrins.[27] However, there is still room for improvement for the porphyrins or other compounds as superior photosensitizers. Some ideal properties, such as low dark toxicity, targeting capabilities (both cellular and subcellular targeting), solubility in aqueous and injectable solutions, reduced nonspecific interactions in biological fluids or cells, are still sought-after. In addition, to increase the water solubility of photosensitizer molecules and improve their delivery into specific tissues or cells, various carriers have been developed for the delivery of the photosensitizers.[28−30] To control better the photoactivity of photosensitizer (PS) and to avoid its damage to healthy tissues and cells, Zheng and co-workers introduced a concept of photodynamic molecular beacons that keep the $^1O_2$ quencher and PS in close proximity through a disease-specific linker to regulate the PDT activity.[31]

Recently, nanographene oxide (NGO) and its derivatives have shown great potential to provide unique and new opportunities for the developments of novel sensors and drug delivery systems.[32−48] Dai and co-workers conjugated polyethylene glycol (PEG) to the NGO's plane and loaded an aromatic anticancer drug via $\pi-\pi$ stacking.[49] The NGO has also been employed as the carrier to deliver PS for PDT.[50,51] Char et al. developed a hyaluronic acid-modified graphene oxide/chlorine e6 nanohybrids for cancer-targeted PDT.[52] Liu and co-workers attached Chlorin e6 (Ce6) onto NGO via supramolecular $\pi-\pi$ stacking, and used it as a photothermally enhanced PDT system.[53] In these NGO-based PDT systems, the release of photosensitizers was accelerated in basic solutions. However, upon cellular internalization by the cells, the nanosystems usually undergo lysosome process.[54] The lysosome system is characterized by low pH (~4.5 to 5.0).[55] Thus, for the nanosized drug delivery systems, the release of their payloads in acidic environment would be more preferable.[56,57]

It is envisioned that a PDT nanosystem with both cellular and mitochondrial targeting as well as pH-sensitive release of PDT agent would be ideal, because these features would effectively enable the system to target specific cells and their mitochondria, release the PDT agent upon being internalized and lead to mitochondrial damage upon light irradiation, and eventually cause the cell apoptosis. Toward this end, in this study, to control the release and phototoxicity of photosensitizer in a more effective manner, we designed a dual-targeting PDT system (with both the cellular and subcellular targeting capability) with a modified NGO as the carrier, as shown in Scheme 1. As for this system, a porphyrin derivative

Scheme 1. Schematic Illustration for the Action of the Dual-Targeting Nanosystem[a]

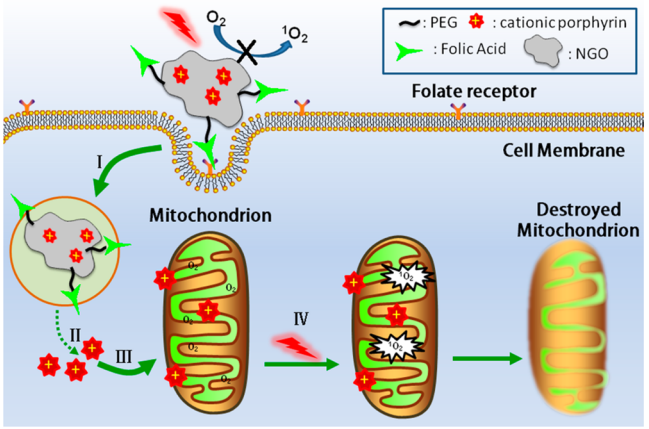

[a]Stage I, folate-receptor-mediated internalization; Stage II, release of photosensitizers under lysosomal pH; Stage III, subcellular localization of photosensitizers in mitochondria; Stage IV, oxidative damage of mitochondrial as a result of singlet oxygen generation under light irradiation.

was synthesized and used as PS, so as to achieve efficient release under acidic environment as well as mitochondria targeting. As the nanocarrier, NGO exhibits multiple purposes: (1) modified with polyethylene glycol (PEG) chains, NGO displays enhanced water dispersibility and biocompatibility; (2) with a folic acid moiety on its surface, the PDT system can specifically target the folate receptor-positive cells, and cause much higher cytotoxicity toward these cells; (3) NGO acts as a quencher for the PS, allowing for lower phototoxicity before the release of PS. Our results indicate that the dual-targeting and the accelerated release of the cationic PS in acidic (lysosomal) environment can achieve enhanced PDT action toward cancer cells.

EXPERIMENTAL DETAILS

Materials. 1,4-dibromobutane, anhydrous K_2CO_3, trimethylamine were purchased from Aladdin Inc. 4-Arm polyethylene glycol-amine was purchased from Yarebio Shanghai. Rhodamine 123, sulfo-*N*-hydroxysuccinimide, and 1-ethyl-3-(3-(dimethylamino)propyl)-carbodiimide hydrochloride were obtained from Aldrich. The bovine serum albumin and RPMI1640 culture media were purchased from Life Technologies. JC-1 (5,5′,6,6′-tetrachloro-1,1′,3,3′-tetrethylbenzimidazolylcarbocyanine iodide) and annexin V-FITC/PI kit were purchased from the Beyotime Institute of Biotechnology. Methanol (MeOH) and *N*,*N*-dimethylformamide (DMF) were distilled before use. All other chemicals were analytical reagents and used without further purification. The water used in this study was the triple-distilled water which was further treated by ion exchange columns and then by a Milli-Q water purification system.

Synthesis of 5-(*p*-(4-Bromo)butoxyphenyl)-10,15,20-triphenylporphyrin (BrTPP) and (5-(*p*-(4-Trimethylammonium)-butoxyphenyl)-10,15,20-triphenylporphyrin Bromide (Mi-

DOI: 10.1021/acsami.5b02297
ACS Appl. Mater. Interfaces 2015, 7, 9287−9296

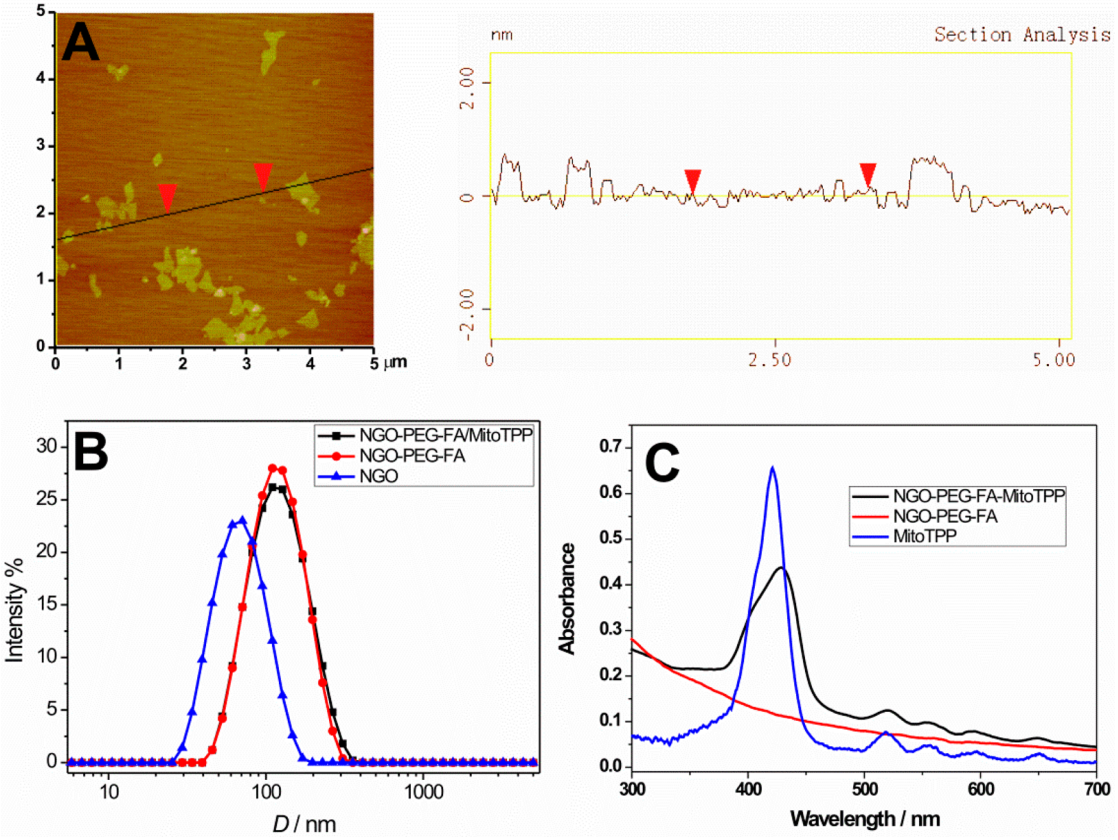

Figure 1. Morphology and spectral properties of NGO-based nanosystems. (A) AFM image for a nanographene oxide (NGO) sample, and the height profile is along the line in the topographic image. (B) Size distribution determined by DLS. (C) Absorption spectra for MitoTPP, NGO-PEG-FA, and MitoTPP-loaded NGO-PEG-FA.

toTPP). The two compounds were synthesized according to a procedure stated in our previous report.[56]

Synthesis of PEGylated Graphene Oxide (NGO-PEG). Graphene oxide (GO) was prepared by adopting a modified Hummer's method utilizing expandable graphite powder;[58] the conjugation of PEG onto graphene oxide was performed according to literature.[53] Briefly, a suspension of carboxylic acid-modified graphene oxide (GO-COOH) (1 mg/mL) was bath-sonicated with 2 mg/mL of 4-arm polyethylene glycol-amine (2 mg/mL) for 5 min. Then, EDC was added in two portions to give a concentration of 5 mmol and the solution was bath-sonicated for another 30 min. After the solution was stirred at room temperature overnight, it was precipitated and rinsed with anhydrous ethanol for five times to remove byproducts and the unreacted chemicals. NGO-PEG was then obtained by centrifugation (15000 r/min) in PBS, the product was purified by dialysis against deionized (DI) water. The black solid NGO-PEG was collected by freeze-drying.

Conjugation of Folic Acid onto NGO-PEG (NGO-PEG-FA). Folic acid (FA, 13 mg, 0.03 mmol), which was treated with EDC (9.6 mg, 0.05 mmol) and sulfo-NHS (10.6 mg, 0.05 mmol) in 5.0 mL of dimethyl sulfoxide (DMSO) under stirring at room temperature for 1 h, was added to the NGO-PEG suspension (50 mL, 1 mg/mL). The mixture was then stirred at room temperature for 24 h in the dark. The solid was precipitated out by addition of methanol and rinsed three times using methanol and then acetone. And the solid was then dissolved in DI water and further purified by dialysis against DI water for 2 days. The product NGO-PEG-FA was collected through freeze-drying.

Preparation of NGO-based PDT Systems (Dual-Targeting Nanosystem NGO-PEG-FA/MitoTPP and the Control NGO-PEG/MitoTPP). 5 mL of 1 mg/mL NGO-PEG-FA (in DI water) was mixed with 1 mg of MitoTPP (in DMSO solution) and stirred overnight at room temperature. Unbound MitoTPP and DMSO were removed by dialyzing against DI water using a dialysis tube (molecular weight cutoff 18 000 Da). The control (NGO-PEG/MitoTPP) was also fabricated with the similar procedure by using NGO-PEG instead.

Determination of Drug Load. For determination of drug load, the dispersion with MitoTPP-loaded NGO system was diluted to a certain concentration, and the absorbance at 420 nm was measured to calculate the content of loaded MitoTPP. Drug load and drug load efficiency were determined as follows

$$\text{drug load (wt\%)} = (\text{weight of loaded drug/weight of NGO}) \times 100\%$$

$$\text{drug load efficiency(\%)} = (\text{weight of loaded drug/weight of drug in feed}) \times 100\%$$

MitoTPP Release From NGO-based Nanosystem in Buffered Solution. In vitro MitoTPP release assays were carried out following the literature procedure.[56,58] The samples were incubated in buffer solutions at pH 7.4 or 5.0 for predetermined time periods and the solutions were then subject to absorbance measurement at 420 nm. The cumulative percentages of released MitoTPP (E_r) were subsequently determined.[56]

Determination of Singlet Oxygen Generation. The singlet oxygen generation of the samples upon light irradiation was conducted using ABDA method.[4] Singlet oxygen generated by the nanosystem oxidizes ABDA and decreases ABDA's absorption. In this study, a suspension of NGO-PEG-FA/MitoTPP (3 mL in pH = 7.4 PBS containing 5 μM MitoTPP) and 10 mM ABDA were stirred in the dark for 30 min, and then subject to light irradiation from a 12W 650 nm LED lamp (light intensity 10 mW/cm^2). At each predetermined time interval, the absorbance at 400 nm for solutions was recorded.

Cell Culture. Two cell lines, HeLa (human cervical cancer cell, FR positive) and L929 (murine aneuploid fibro-sarcoma cell, FR negative)

DOI: 10.1021/acsami.5b02297
ACS Appl. Mater. Interfaces 2015, 7, 9287−9296

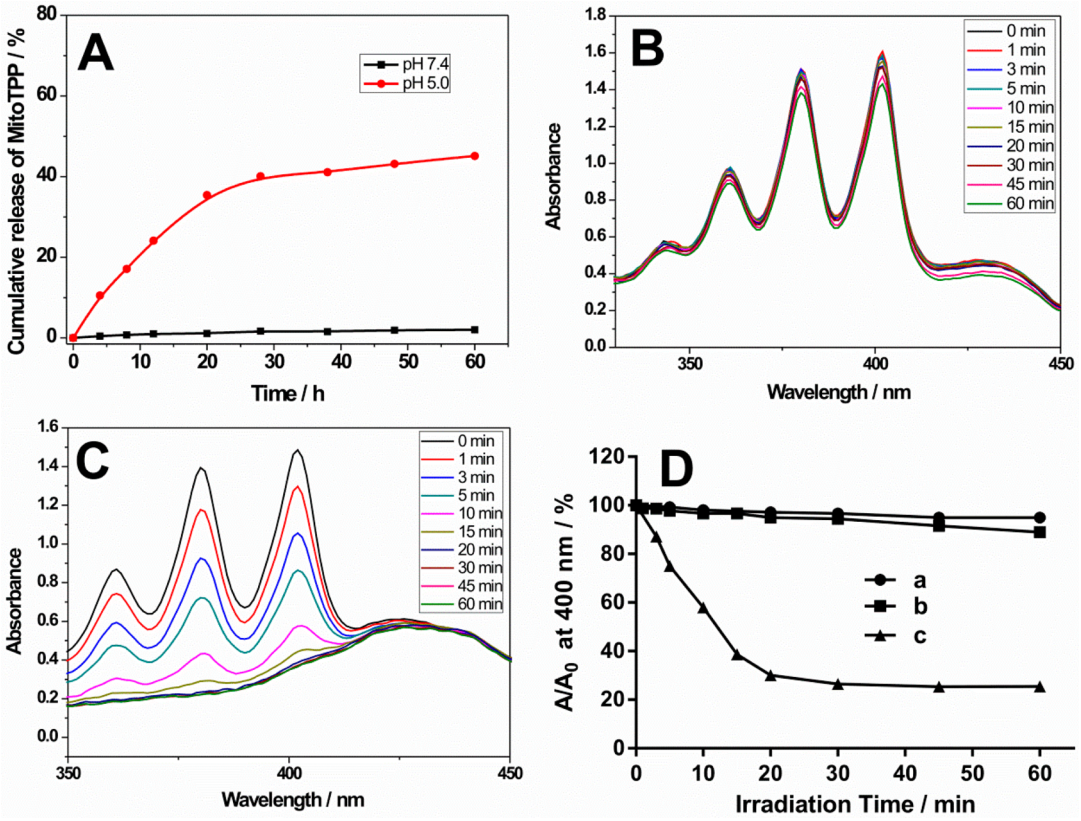

Figure 2. (A) Release profile of MitoTPP from NGO-PEG-FA/MitoTPP samples at 37 °C in aqueous media. (B and C) Absorption spectra for ABDA in the presence of NGO-PEG-FA/MitoTPP over different periods of time under irradiation. The samples were treated with pH 7.4 PBS buffer (B) or pH 5.0 acetate buffer (C) for 8 h before the measurement. (D) Absorbance values for ABDA at 400 nm plotted against irradiation time in the absence of NGO-PEG-FA/MitoTPP (curve a) and in the presence of NGO-PEG-FA/MitoTPP samples upon being treated with pH = 7.4 (curve b) or pH = 5.0 (curve c) buffers.

were incubated in FA-free RPMI 1640 medium supplemented with 10% fetal bovine serum (FBS) (penicillin/streptomycin 100 U/mL) at 37 °C with 5% CO_2.

Cellular Uptake and Colocalization Imaging. Cell uptake and localization were observed on a confocal laser scanning microscope. The colocalization imaging experiments were performed with a procedure according to our previous report[16] except that the photosensitizer (MitoTPP) was excited at 405 nm.

Apoptosis Analysis by Annexin V-FITC/Propidium Iodide (PI) Dual Staining. HeLa cells were used to evaluate the pro-apoptotic effect of the NGO-based nanosystems, and the analysis was conducted following our previously reported procedure.[16]

Mitochondrial Membrane Potential. Change in mitochondrial membrane potential for HeLa cells were monitored using a fluorescent probe JC-1.[16]

Dark cytotoxicity and Phototoxicity. The cytotoxicity caused by the samples in the dark or upon light irradiation was evaluated using cell viability assays. The cell viability of HeLa and L929 cells exposed to MitoTPP, BrTPP, NGO-PEG-FA/MitoTPP, or NGO-PEG/MitoTPP were assessed by MTT assay. The procedure for the analysis is the same as that reported elsewhere.[56] In this study, a 12W LED lamp with 10 mW/cm^2 light intensity and 650 nm wavelength was used to generate irradiation light for PDT effect.

Instrumentation. Fluorescence spectra and UV−vis spectra were recorded on a Hitachi F-4600 fluorescence spectrophotometer and a Hitachi U-3010 UV−vis spectrophotometer, respectively. ^{1}H NMR spectra were recorded on a Bruker Avance 400 MHz NMR spectrometer. A Leica TCS-SP5 confocal microscope was used for cell imaging. Atomic-force microscopy (AFM) images were obtained using a DI Veeko Multimode V atomic force microscope. Dynamic light scattering (DLS) measurement was carried out on a Mavern Nanosizer. Flow cytometry were recorded on Beckman Coulter Epics XL.

RESULTS AND DISCUSSION

Preparation of Dual-Targeting PDT System with NGO-PEG-FA as the Carrier. In this study, the PEG- and folic acid-modified NGO were prepared according to the procedures stated in the Experimental Section; their ^{1}H NMR and absorption spectrum are given in Figures S1 and S2 of the Supporting Information. The cationic porphyrin (MitoTPP) was synthesized as shown in Scheme S1 pf the Supporting Information, and its ^{1}H NMR, MS, and absorption spectra are shown in Figures S3−S5 in the Supporting Information. The loading of MitoTPP onto NGO-PEG-FA was conducted by mixing NGO-PEG-FA and MitoTPP in aqueous solution overnight under controlled pH. The load of MitoTPP was quantified by calculating the absorption band of porphyrins at 420 nm over the NGO background (Figure 1C and Figure S6 of the Supporting Information); the load of MitoTPP in NGO-PEG-FA was determined as 37.2 wt %.

The morphology of NGO was characterized by AFM (Figure 1a), which indicates that the NGO exists in the sheet-like shapes. The thickness, measured from the height profile of AFM image is about 1 nm, indicating the formation of the single-layered NGO. On the other hand, the size distribution determined by DLS for the as-prepared and modified NGO is given in Figure 1b, which indicates an increase in NGO's size upon modification.

DOI: 10.1021/acsami.5b02297
ACS Appl. Mater. Interfaces 2015, 7, 9287−9296

In Vitro Release of MitoTPP from Its Carrier. To investigate the release of MitoTPP from NGO, the NGO-PEG-FA/MitoTPP samples were incubated in a simulated physiological solution (PBS, pH 7.4) and in acidic environment (acetate buffer, pH 5.0) at 37 °C. The released amount of photosensitizer was determined by absorbance measurements at 420 nm. The release profiles illustrated in Figure 2A suggest that the release behavior of the photosensitizer from the NGO-based systems is strongly dependent on the releasing time and pH. MitoTPP-loaded NGO shows a much faster release rate at pH 5.0. Under neutral pH, many carboxyl groups (−COOH) on NGO exist as the ionized carboxyl groups ($-COO^-$), which have strong electrostatic attraction with the cationic quaternary ammoniums in MitoTPP. Hence, the electrostatic attraction and the $\pi-\pi$ stacking make MitoTPP bind strongly on NGO. Under acidic pH, the ionized carboxyl groups turns into the nonionized ones (−COOH), making the electrostatic attraction much weaker and promoting the release of MitoTPP from NGO. This pH-dependent releasing behavior is beneficial for the PS to escape from the acidic endosome/lysosome compartments and then diffuse into mitochondria.

Singlet Oxygen ($^1O_2$) Generation under Two Different pH Values. Singlet oxygen ($^1O_2$), the first excited electronic state of molecular oxygen, plays an important role in mechanisms of cell death.[59] It is highly reactive and can damage organic materials and biological tissues. NGO and its derivatives have been reported to have the capability to quench the phototoxicity of PS by fluorescence resonance energy transfer (FRET).[50,60] To verify the difference in the $^1O_2$ generation capacity for the NGO-PEG-FA/MitoTPP at two pHs, 9,10-anthracenediylbis(methylene)dimalonic acid (ABDA) indicator was used to determine $^1O_2$ production.[61] The absorption spectra for ABDA in NGO-PEG-FA/MitoTPP dispersion (pH 7.4 or pH 5.0) with increasing exposure time are presented in Figure 2B,C, respectively; and the variation of absorbance for ABDA are shown in Figure 2D. As we can see from the figures, upon being treated by pH 7.4 buffer solution and under light irradiation, the absorbance for ABDA in NGO-PEG-FA/MitoTPP dispersion changes very little; while upon being treated with acidic buffer (pH 5.0), ABDA is found substantially photobleached within the initial 15 min irradiation. In contrast, a control experiment shows that ABDA is barely bleached in the absence of the photosensitizer (curve a, Figure 2D). The results indicate that, NGO-PEG-FA can act as a singlet oxygen quencher when the MitoTPP is loaded onto it, and the positively charged porphyrin derivative can efficiently produces $^1O_2$ under light irradiation after being released from its carrier in acidic environment.

Dual-Targeting Capability of NGO-PEG-FA/MitoTPP System. The cellular and mitochondrial targeting capability for the NGO-based samples was investigated using fluorescent microscopy. First, to verify the cellular targeting capacity, HeLa cell (FR-positive) and L929 cell (FR-negative, the control) were incubated with NGO-PEG-FA/MitoTPP respectively; and the results of the cellular uptake at varied time periods are shown in Figure 3. After 8 h of incubation, the weak intracellular fluorescence suggests that few NGO-PEG-FA/MitoTPP nanosystems are internalized by L929 cells; while HeLa cells exhibit much stronger red fluorescence (corresponding to the fluorescence of MitoTPP molecules released from NGO), indicating that far more NGO-PEG-FA/MitoTPP are internalized into HeLa cells than those into L929 cells. At longer incubation time (20 h), the fluorescence in both cell lines becomes more prominent, but the HeLa cells still display much stronger intracellular fluorescence. These results demonstrate that, incorporting folic acid onto NGO-based nanosystem can enhance the cellular uptake for FR-positive cells. On the other hand, we also recorded the intracellular fluorescence for HeLa cells incubated with either NGO-PEG-FA/MitoTPP or NGO-PEG/MitoTPP for a certain period of time, and the result is presented in Figure S7 in the Supporting Information. As one can see from the figure, upon 8 h of incubation, the cells treated with the NGO system containing FA (NGO-PEG-FA/MitoTPP) exhibit much brighter fluorescence than those treated with the NGO system without FA (NGO-PEG/MitoTPP), and this may provide additional evidence for the cellular targeting capability of NGO-PEG-FA/MitoTPP.

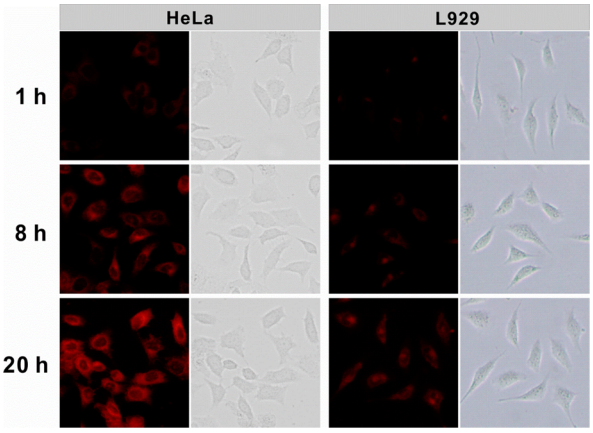

Figure 3. Fluorescence microscopic images for HeLa and L929 cells incubated with NGO-PEG-FA/MitoTPP at varied time periods in folic acid-free RPMI 1640 medium.

To track the release and mitochondrial localization of the PDT systems, costaining experiments using a PDT system and a mitochondrion-specific dye (rhodamine 123, Rh123 for short) were performed. First, we investigated the subcellular localization of the molecular porphyrins (MitoTPP and BrTPP) in HeLa cells using confocal microscopy, as shown in Figure S8 of the Supporting Information. The preferential site of intracellular localization for MitoTPP has been found to be the mitochondria, as evidenced by the perfect overlap of porphyrin fluorescence (red) and Rh123 fluorescence (green); the nontargeting porphyrin (BrTPP) displays poor colocalization with Rh123. Figure 4 shows the fluorescent patterns for NGO-PEG-FA/MitoTPP and their overlay with the Rh123. It can be seen from the images that, at 1 h of incubation, very dim fluorescence can be observed, indicating the majority of MitoTPPs have not been released from their carriers yet, as NGO can quench the fluorescence of porphyrins (Figure S9 of the Supporting Information); at 8 h of incubation, some red fluorescent dots are found inside cells, which may suggest some of the MitoTPP molecules have been released from the NGO carriers. And upon longer incubation (20 h), much stronger red fluorescence can be observed; more importantly, the fluorescence signals from Rh123 and porphyrin match well and obvious yellow fluorescence (overlapping regions of red and green) can be found in the mitochondria, demonstrating the mitochondria targeting ability of molecular MitoTPP upon being released from their carriers. The MitoTPP can target the mitochondria due to the presence of the lipophilic cation that can facilitate its release and accumulation in mitochondria.

DOI: 10.1021/acsami.5b02297
ACS Appl. Mater. Interfaces 2015, 7, 9287−9296

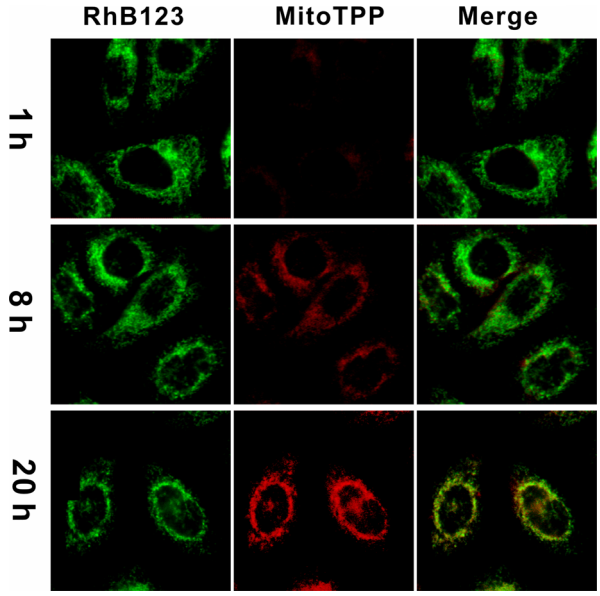

Figure 4. Confocal microscopic images of HeLa cells costained with NGO-PEG-FA/MitoTPP and rhodamine 123 at varied time periods in FA-free RPMI 1640 medium.

Mitochondria Damage Induced by PDT. The PDT effect can induce mitochondrial damage and the subsequent apoptosis of cells. In this study, a membrane-permeant dye (JC-1) was used to monitor mitochondrial status upon singlet oxygen treatment. The loss of mitochondrial membrane potential ($\Delta\Psi$, a hallmark of cytochrome c translocation and the start of the apoptotic process) is an key indicator to evaluate the dysfunction of mitochondria, because the damaging of mitochondria causes the substantial loss of its membrane potential.[62,63] The JC-1 dye undergoes a reversible change in fluorescence emission, cells with high mitochondrial membrane potential facilitate the formation of dye aggregates, which exhibit red fluorescence; cells with low potential will contain monomeric JC-1 and display green fluorescence. Therefore, the red/green emission ratio can help to determine the status of mitochondria and cells; and we could distinguish live cells from damaged ones by following the singlet oxygen treatment by recording the fluorescence change of JC-1 using confocal microscopy and flow cytometry.

Figure 5 shows the representative results of JC-1 assays for HeLa cells as a result of singlet oxygen treatment (i.e., incubation with PDT system followed by light irradiation). Confocal microscopy reveals that in unirradiated HeLa cells (0 min), well-polarized mitochondria are marked by both punctate red and green fluorescent staining. However, treatment with both forms of PDT systems (NGO-PEG/MitoTPP and NGO-PEG-FA/MitoTPP) and then exposure to light causes changes in cell staining: the red emission regions gradually decrease with the increasing irradiation time, while green emission intensity in the cytoplasm increases. It is noteworthy that the enhancement of green fluorescence in the cytoplasm is more pronounced when the cells are treated with the dual-targeting PDT system (NGO-PEG-FA/MitoTPP), and upon irradiation for 30 min, most of red dot-like fluorescent images turn into the diffusive green fluorescence (Figure 5A). These results indicate that, the singlet oxygen treatment can lead to the mitochondria damage; and the PDT system with folic acid ligand on its surface (NGO-PEG-FA/MitoTPP) can damage the mitochondria more efficiently (Figure 5A,B), which can be ascribed to the fact that more NGO-PEG-FA/MitoTPP nanohybrids have been internalized by FR-positive HeLa cells than NGO-PEG/MitoTPP.

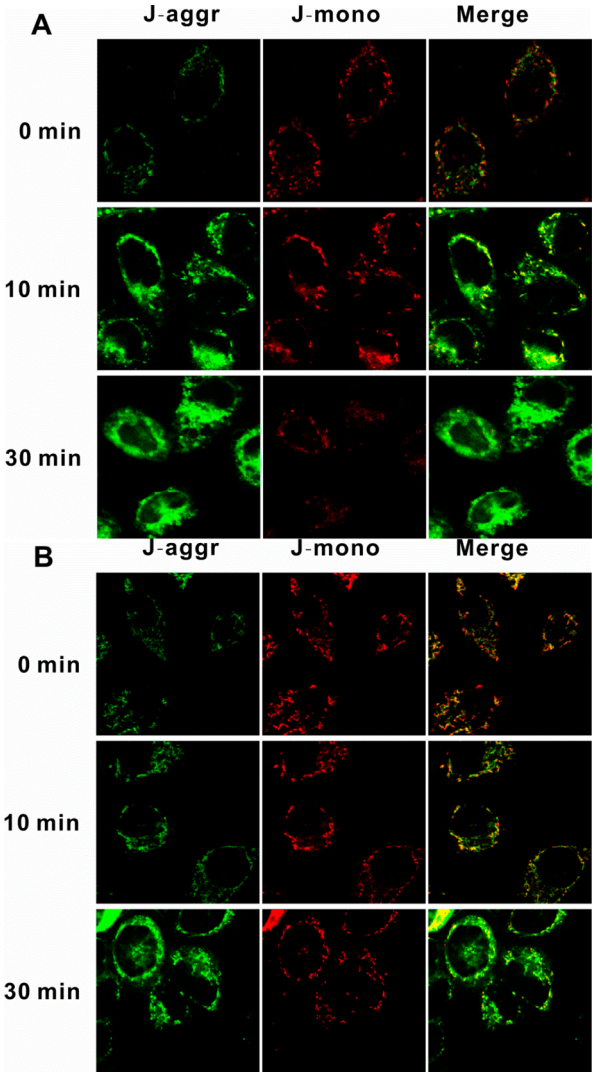

Figure 5. Confocal microscopic images of HeLa cells treated with NGO-PEG-FA/MitoTPP (A) or NGO-PEG/MitoTPP (B) and then stained with 1 μg/mL JC-1. The cells were incubated with the NGO-based PDT systems (equivalent to about 5 μM MitoTPP) for 8 h and then exposed to 12 W LED (650 nm) light irradiation for 0, 10, or 30 min, respectively.

We also measured the change in population of cells of different fluorescence upon $^1O_2$ treatment using flow cytometry. Analysis of the cells by flow cytometry (Figure 6(I)) reveals a decrease in red fluorescence (FL2 channel, the vertical coordinate) after the treatment. As one can see from the figure, before nanosystem treatement, high $\Delta\Psi$ cells predominate in the cell population. Upon treatment with the nanosystem, remarkable increases in low $\Delta\Psi$ cells are recorded (in a dose-dependent manner), which provides additional evidence for the effectiveness of the NGO-based system on mitochondria damage.

Cytotoxicity Caused by PDT. The flow cytometric analysis of the annexin V/PI labeling assay was utilized to evaluate efficacy of the dual-targeted PDT system in cell apoptosis/death. For this purpose, HeLa cells treated with

DOI: 10.1021/acsami.5b02297
ACS Appl. Mater. Interfaces 2015, 7, 9287−9296

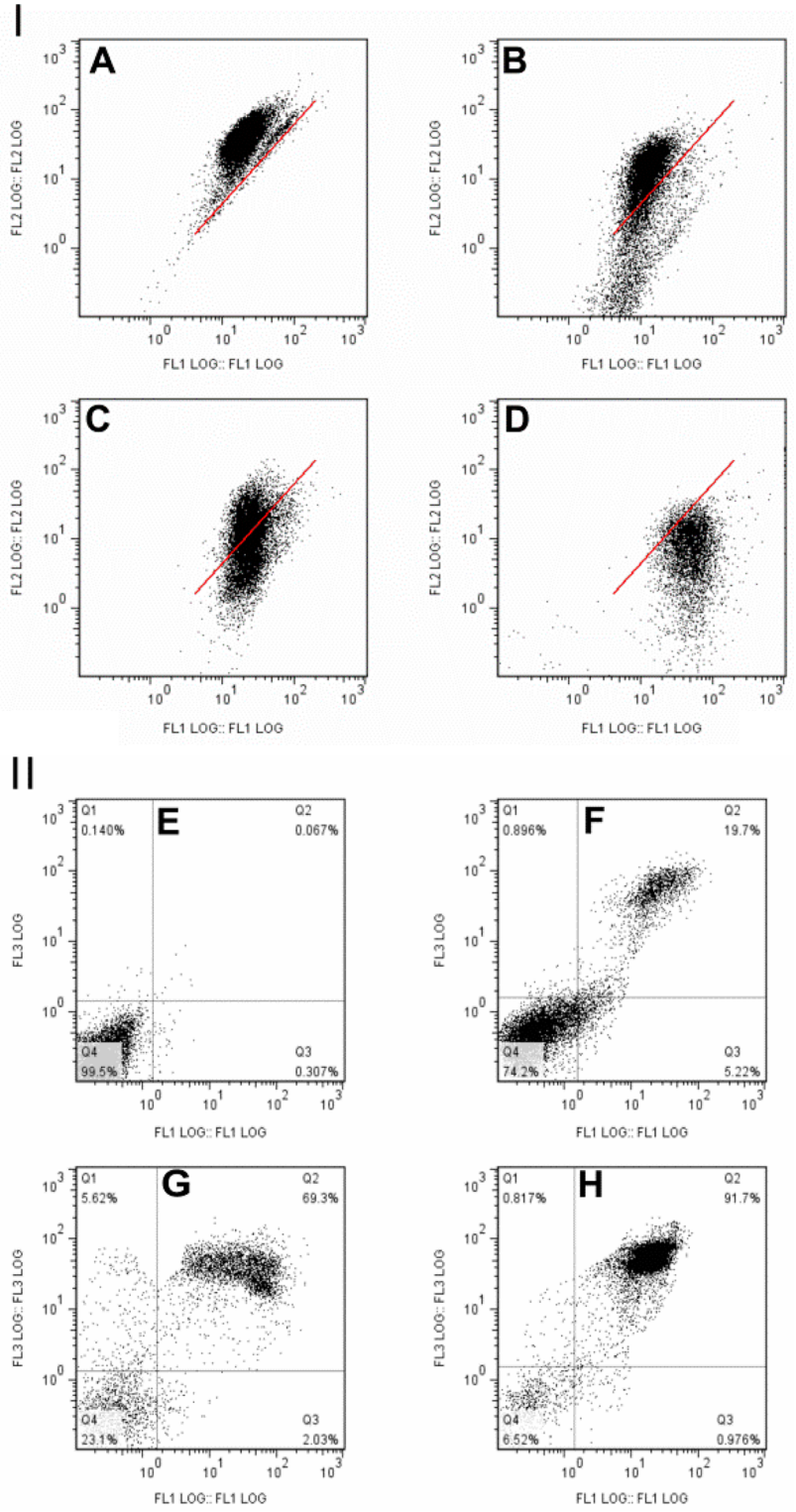

Figure 6. (I) Typical flow cytometric analyses (with JC-1 as indicator) for HeLa cells treated with NGO-PEG-FA/MitoTPP for 8 h before exposure to 12 W LED irradiation for 30 min at the MitoTPP concentration of 0 μM (A), 1 μM (B), 3 μM (C) and 5 μM (D). Red lines separate vital cells and apoptotic cells. (II) Typical percent distribution of HeLa cells obtained using annexin V-FITC/PI staining experiments. Cells were treated with NGO-PEG-FA/MitoTPP before measurement. (E) 0 μM (control); (F) 1 μM; (G) 3 μM, and (H) 5 μM. The samples were exposed to 12 W LED for 30 min after 8 h incubation with the dual-targeting nanosystem.

various amounts of NGO-PEG-FA/MitoTPP were exposed to light irradiation for 30 min. Figure 6(II) shows the typical results of the assay, and the cytogram in the figure presents the bivariate annexin V/PI analysis of the HeLa cell suspensions. Vital cells are negative for both PI and annexin V (in Q4), early apoptotic cells are PI negative and annexin V positive (Q3), late apoptotic/dead cells are positive for both PI and annexin V (Q4), while the damaged cells located in region Q1.

As can be seen from Figure 6(II) E, the negative control (without being treated by the NGO-based PDT system)

DOI: 10.1021/acsami.5b02297
ACS Appl. Mater. Interfaces 2015, 7, 9287−9296

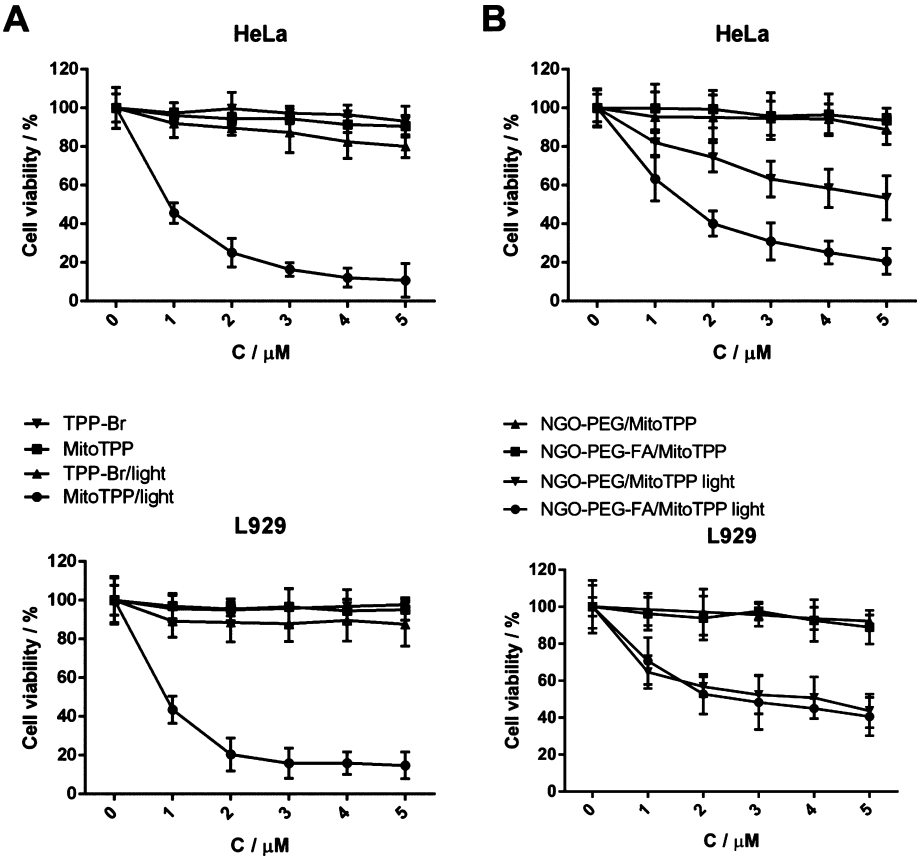

Figure 7. Viability of two cell lines (HeLa and L929) upon treatment with molecular porphyrins (A) and NGO-based porphyrin systems (B). *C* denotes the molar concentration of porphyrin moieties in the media. All the culture media used in this system were folic acid free. Three independent experiments were conducted, each with sets of eight replicates. Data represent mean ± SD from three independent experiments.

exhibits high percentage (99.5%) of vital cells; upon treatment with the dual-targeting nanosystems and exposure to light irradiation, the percentage of vital cells declines, and that for the late apoptotic/dead cells increases gradually in a concentration-dependent way. For the cells treated with high concentration of NGO-PEG-FA/MitoTPP (with 5 μM MitoTPP), the percentage of late apoptotic/dead cells increases to as high as 91.7%, indicating the dual-targeted PDT-based system can provide efficient apoptosis action for the FR-positive cells.

We also performed MTT assays for two cell lines (L929 and HeLa) upon treatment with different PDT systems (Figure 7). First, we investigated the cell viability for the two cell lines treated by molecular photosensitizers, i.e. the mitochondria-targeting photosensitizer MitoTPP and the nontargeting one BrTPP, as shown in Figure 7A. Cell death is not observed when untreated cells (0 μM photosensitizer) are irradiated with light or not. Moreover, no significant dark toxicity can be observed in cells treated with up to 5 μM of either BrTPP or MitoTPP. This is probably because of their incapability to produce singlet oxygen in the dark. Upon light irradiation for 30 min, both cell lines treated by MitoTPP show significant phototoxicity; while slight phototoxicity is observed in cells treated with BrTPP. Presumably, in addition to its nontargeted nature, the low solubility of BrTPP in the culture media might also contribute to the low cytotoxicity toward the cells.

As for the viability for the cells treated by the NGO-based PDT systems, HeLa cells treated with either NGO-PEG/MitoTPP or NGO-PEG-FA/MitoTPP exhibit almost no dark toxicity, as shown in Figure 7B. After 8 h of incubation with the nanosystem followed by 30 min of light irradiation, the cell viability of diminishes, and the reducing in cell viability is found dependent on both the photosensitizer concentration and the type of its carrier. For the FR-negative L929 cells, treatment with NGO-PEG/MitoTPP or NGO-PEG-FA/MitoTPP causes similar phototoxicity; while for the FR-positive HeLa cells, the folic acid-modified system (NGO-PEG-FA/MitoTPP) causes much higher phototoxicity than the system with no FA modification, as shown in Figure 7B. In addition, the cell viabilities only treated by the light is presented in Figure S10 of the Supporting Information, which proves that the light irradiation alone could not reduce the viability of the cells. We also determined the cell viability for a FR-negative cancer cell line (A549), and the results are shown in Figure S11 of the Supporting Information, which demonstrate that the treatment with NGO-PEG/MitoTPP or NGO-PEG-FA/MitoTPP causes similar phototoxicity. This provides additional evidence that the incorporation of folic acid onto NGO-based PDT system can offer enhanced phototoxicity toward FR-positive cancer cells.

CONCLUSIONS

A dual-targeting (cellular targeting and subcellular targeting) PDT nanosystem has been successfully prepared by loading a cationic porphyrin (MitoTPP) onto the surface of a folic acid-modified NGO through electrostatic interaction and $\pi-\pi$ stacking. The NGO-based carrier can quench both fluorescence and singlet oxygen generation of MitoTPP, and can also target FR-positive cancer cells and release its cargo (MitoTPP) upon being internalized. The released MitoTPP can subsequently

DOI: 10.1021/acsami.5b02297
ACS Appl. Mater. Interfaces 2015, 7, 9287−9296

accumulate in mitochondria and exert its PDT action. The dual-targeting system can efficiently cause mitochondrial damage upon light irradiation, as evidenced by the loss of the mitochondrial membrane potential, and eventually leads to the death of cancer cells.

■ ASSOCIATED CONTENT

Supporting Information

Synthetic route of the mitochondria targeting photosensitizer MitoTPP, ^{1}H NMR spectrum for the NGO-PEG-FA in D_2O, absorption spectra for the aqueous dispersions of NGO-PEG and NGO-PEG-FA, ^{1}H NMR and mass spectra for the BrTPP, ^{1}H NMR and mass spectra for the MitoTPP, UV−vis spectra of MitoTPP in water, relationship between concentration for MitoTPP and their absorbance, fluorescence microscope images for HeLa cells incubated with NGO-PEG-FA/MitoTPP or NGO-PEG/MitoTPP for 8 h in the FA-free RPMI 1640 medium, CLSM of HeLa cells incubated with porphyrins (MitoTPP or BrTPP) and rhodamine 123 for 2 h, fluorescence spectra for MitoTPP and NGO-PEG-FA/MitoTPP with the same concentration of MitoTPP, viability assay for two untreated (by nanosystem) cells incubated for 24 h in dark or under continuous light irradiation using a 12 W LED lamp (650 nm), and viability assessed by MTT assay for A549 cell line (a FR-negative cancer cell) treated with different NGO-based porphyrin systems. This material is available free of charge via the Internet at http://pubs.acs.org.

■ AUTHOR INFORMATION

Corresponding Authors

*F. Zeng. E-mail: mcfzeng@scut.edu.cn.
*S. Wu. E-mail: shzhwu@scut.edu.cn.

Notes

The authors declare no competing financial interest.

■ ACKNOWLEDGMENTS

We gratefully acknowledge the financial support by NSFC (21474031, 21174040 and 21025415), the National Key Basic Research Program of China (Project No. 2013CB834702), and "the Fundamental Research Funds for the Central Universities, SCUT".

■ REFERENCES

(1) Celli, J. P.; Spring, B. Q.; Rizvi, I.; Evans, C. L.; Samkoe, K. S.; Verma, S.; Pogue, B. W.; Hasan, T. Imaging and Photodynamic Therapy: Mechanisms, Monitoring, and Optimization. *Chem. Rev.* **2010**, *110*, 2795−2838.

(2) Dolmans, D. E.; Fukumura, D.; Jain, R. K. Photodynamic Therapy for Cancer. *Nat. Rev. Cancer* **2003**, *3*, 380−387.

(3) Lovell, J. F.; Liu, T. W.; Chen, J.; Zheng, G. Activatable Photosensitizers for Imaging and Therapy. *Chem. Rev.* **2010**, *110*, 2839−2857.

(4) Zhao, T.; Yu, K.; Li, L.; Zhang, T.; Guan, Z.; Gao, N.; Yuan, P.; Li, S.; Yao, S. Q.; Xu, Q.-H.; Xu, G. Q. Gold Nanorod Enhanced Two-Photon Excitation Fluorescence of Photosensitizers for Two-Photon Imaging and Photodynamic Therapy. *ACS Appl. Mater. Interfaces* **2014**, *6*, 2700−2708.

(5) Henderson, B. W.; Dougherty, T. J. How Does Photodynamic Therapy Work? *Photochem. Photobiol.* **1992**, *55*, 145−157.

(6) Castano, A. P.; Mroz, P.; Hamblin, M. R. Photodynamic Therapy and Anti-tumour Immunity. *Nat. Rev. Cancer* **2006**, *6*, 535−545.

(7) Zheng, G.; Chen, J.; Stefflova, K.; Jarvi, M.; Li, H.; Wilson, B. C. Photodynamic Molecular Beacon as an Activatable Photosensitizer Based on Protease-Controlled Singlet Oxygen Quenching and Activation. *Proc. Natl. Acad. Sci. U. S. A.* **2007**, *104*, 8989−8994.

(8) Lucky, S. S.; Soo, K. C.; Zhang, Y. Nanoparticles in photodynamic therapy. *Chem. Rev.* **2015**, *115*, 1990−2042.

(9) Rajaputra, P.; Nkepang, G.; Watley, R.; You, Y. Synthesis and in Vitro Biological Evaluation of Lipophilic Cation Conjugated Photosensitizers for Targeting Mitochondria. *Bioorg. Med. Chem.* **2013**, *21*, 379−387.

(10) Akimoto, J.; Haraoka, J.; Aizawa, K. Preliminary Clinical Report on Safety and Efficacy of Photodynamic Therapy Using Talaporfin Sodium for Malignant Gliomas. *Photodiagn. Photodyn. Ther.* **2012**, *9*, 91−99.

(11) Ormond, A.; Freeman, H. Dye Sensitizers for Photodynamic Therapy. *Materials* **2013**, *6*, 817−840.

(12) Fulda, S.; Galluzzi, L.; Kroemer, G. Targeting Mitochondria for Cancer Therapy. *Nat. Rev. Drug Discovery* **2010**, *9*, 447−464.

(13) Murphy, M. P.; Smith, R. A. Targeting Antioxidants to Mitochondria by Conjugation to Lipophilic Cations. *Annu. Rev. Pharmacol. Toxicol.* **2007**, *47*, 629−656.

(14) Zhou, F.; Wu, S.; Yuan, Y.; Chen, W. R.; Xing, D. Mitochondria-Targeting Photoacoustic Therapy Using Single-Walled Carbon Nanotubes. *Small* **2012**, *8*, 1543−1550.

(15) Shi, Y. A Structural View of Mitochondria-Mediated Apoptosis. *Nat. Struct. Mol. Biol.* **2001**, *8*, 394−401.

(16) Xu, J.; Zeng, F.; Wu, H.; Hu, C.; Yu, C.; Wu, S. Preparation of a Mitochondria-Targeted and NO-Releasing Nanoplatform and its Enhanced Pro-Apoptotic Effect on Cancer Cells. *Small* **2014**, *10*, 3750−3760.

(17) Du, F.; Min, Y.; Zeng, F.; Yu, C.; Wu, S. A Targeted and FRET-based Ratiometric Fluorescent Nanoprobe for Imaging Mitochondrial Hydrogen Peroxide in Living Cells. *Small* **2014**, *10*, 964−972.

(18) Frantz, M. C.; Wipf, P. Mitochondria as a Target in Treatment. *Environ. Mol. Mutagen.* **2010**, *51*, 462−475.

(19) Leiris, S.; Lucas, M.; Dupuy d'Angeac, A.; Morère, A. Synthesis and Biological Evaluation of Cyclic Nitrogen Mustards Based on Carnitine Framework. *Eur. J. Med. Chem.* **2010**, *45*, 4140−4148.

(20) Faissat, L.; Martin, K.; Chavis, C.; Montéro, J.-L.; Lucas, M. New Nitrogen Mustards Structurally Related to (l)-Carnitine. *Bioorg. Med. Chem.* **2003**, *11*, 325−334.

(21) Sheu, S.-S.; Nauduri, D.; Anders, M. W. Targeting Antioxidants to Mitochondria: A New Therapeutic Direction. *Biochim. Biophys. Acta, Mol. Basis Dis.* **2006**, *1762*, 256−265.

(22) Zhang, H.; Han, Y.; Guo, Y.; Dong, C. Porphyrin Functionalized Graphene Nanosheets-based Electrochemical Aptasensor for Label-Free ATP Detection. *J. Mater. Chem.* **2012**, *22*, 23900−23905.

(23) Ethirajan, M.; Chen, Y.; Joshi, P.; Pandey, R. K. The Role of Porphyrin Chemistry in Tumor Imaging and Photodynamic Therapy. *Chem. Soc. Rev.* **2011**, *40*, 340−362.

(24) Xing, C.; Yang, G.; Liu, L.; Yang, Q.; Lv, F.; Wang, S. Conjugated Polymers for Light-Activated Antifungal Activity. *Small* **2012**, *8*, 524−529.

(25) Alvarez, M. G.; Principe, F.; Milanesio, M. E.; Durantini, E. N.; Rivarola, V. Photodynamic Damages Induced by a Monocationic Porphyrin Derivative in a Human Carcinoma Cell Line. *Int. J. Biochem. Cell Biol.* **2005**, *37*, 2504−2512.

(26) Ngen, E. J.; Rajaputra, P.; You, Y. Evaluation of Delocalized Lipophilic Cationic Dyes as Delivery Vehicles for Photosensitizers to Mitochondria. *Bioorg. Med. Chem.* **2009**, *17*, 6631−6640.

(27) Lei, W.; Xie, J.; Hou, Y.; Jiang, G.; Zhang, H.; Wang, P.; Wang, X.; Zhang, B. Mitochondria-Targeting Properties and Photodynamic Activities of Porphyrin Derivatives Bearing Cationic Pendant. *J. Photochem. Photobiol., B* **2010**, *98*, 167−171.

(28) Chen, C.; Zhou, L.; Geng, J.; Ren, J.; Qu, X. Photosensitizer-Incorporated Quadruplex DNA-Gated Nanovechicles for Light-Triggered, Targeted Dual Drug Delivery to Cancer Cells. *Small* **2013**, *9*, 2793−2800.

(29) Barreto, J. A.; O'Malley, W.; Kubeil, M.; Graham, B.; Stephan, H.; Spiccia, L. Nanomaterials: Applications in Cancer Imaging and Therapy. *Adv. Mater.* **2011**, *23*, 18−40.

DOI: 10.1021/acsami.5b02297
ACS Appl. Mater. Interfaces 2015, 7, 9287−9296

(30) Zhang, Z.; Liu, C.; Bai, J.; Wu, C.; Xiao, Y.; Li, Y.; Zheng, J.; Yang, R.; Tan, W. Silver Nanoparticle-Gated Mesoporous Silica-Coated Gold Nanorods (AuNR@MS@AgNPs): Low Premature Release and Multifunctional Cancer Theranostic Platform. *ACS Appl. Mater. Interfaces* **2015**, *7*, 6211−6219.
(31) Chen, J.; Stefflova, K.; Niedre, M. J.; Wilson, B. C.; Chance, B.; Glickson, J. D.; Zheng, G. Protease-Triggered Photosensitizing Beacon Based on Singlet Oxygen Quenching and Activation. *J. Am. Chem. Soc.* **2004**, *126*, 11450−11451.
(32) Baptista-Pires, L.; Pérez-López, B.; Mayorga-Martinez, C. C.; Morales-Narváez, E.; Domingo, N.; Esplandiu, M. J.; Alzina, F.; Torres, C. M. S.; Merkoçi, A. Electrocatalytic Tuning of Biosensing Response Through Electrostatic or Hydrophobic Enzyme−Graphene Oxide Interactions. *Biosens. Bioelectron.* **2014**, *61*, 655−662.
(33) Yang, K.; Feng, L.; Shi, X.; Liu, Z. Nano-Graphene in Biomedicine: Theranostic Applications. *Chem. Soc. Rev.* **2013**, *42*, 530−547.
(34) Morales-Narváez, E.; Merkoçi, A. Graphene Oxide as an Optical Biosensing Platform. *Adv. Mater.* **2012**, *24*, 3298−3308.
(35) Georgakilas, V.; Otyepka, M.; Bourlinos, A. B.; Chandra, V.; Kim, N.; Kemp, K. C.; Hobza, P.; Zboril, R.; Kim, K. S. Functionalization of Graphene: Covalent and Non-Covalent Approaches, Derivatives and Applications. *Chem. Rev.* **2012**, *112*, 6156−6214.
(36) Feng, L. Z.; Li, K. Y.; Shi, X. Z.; Gao, M.; Liu, J.; Liu, Z. Smart pH-Responsive Nanocarriers Based on Nano-Graphene Oxide for Combined Chemo- and Photothermal Therapy Overcoming Drug Resistance. *Adv. Healthcare Mater.* **2014**, *3*, 1261−1271.
(37) Xu, X.; Huang, J.; Li, J.; Yan, J.; Qin, J.; Li, Z. A Graphene Oxide-based AIE Biosensor with High Selectivity toward Bovine Serum Albumin. *Chem. Commun.* **2011**, *47*, 12385−12387.
(38) Shen, H.; Zhang, L. M.; Liu, M.; Zhang, Z. J. Biomedical Applications of Graphene. *Theranostics* **2012**, *2*, 283−294.
(39) Zhang, L. M.; Lu, Z. X.; Zhao, Q. H.; Huang, J.; Shen, H.; Zhang, Z. J. Enhanced Chemotherapy Efficacy by Sequential Delivery of siRNA and Anticancer Drugs Using PEI-Grafted Graphene Oxide. *Small* **2011**, *7*, 460−464.
(40) Yang, X.; Zhang, X.; Ma, Y.; Huang, Y.; Wang, Y.; Chen, Y. Superparamagnetic Graphene Oxide-Fe_3O_4 Nanoparticles Hybrid for Controlled Targeted Drug Carriers. *J. Mater. Chem.* **2009**, *19*, 2710−2714.
(41) Xing, F.; Meng, G.-X.; Zhang, Q.; Pan, L.-T.; Wang, P.; Liu, Z.-B.; Jiang, W.-S.; Chen, Y.; Tian, J.-G. Ultrasensitive Flow Sensing of a Single Cell Using Graphene-based Optical Sensors. *Nano Lett.* **2014**, *14*, 3563−3569.
(42) Kumar, R.; Jayaramulu, K.; Maji, T. K.; Rao, C. N. R. Hybrid Nanocomposites of ZIF-8 with Graphene Oxide Exhibiting Tunable Morphology, Significant CO_2 Uptake and Other Novel Properties. *Chem. Commun.* **2013**, *49*, 4947−4949.
(43) Xue, T.; Peng, B.; Xue, M.; Zhong, X.; Chiu, C.-Y.; Yang, S.; Qu, Y.; Ruan, L.; Jiang, S.; Dubin, S.; Kaner, R. B.; Zink, J. I.; Meyerhoff, M. E.; Duan, X.; Huang, Y. Integration of Molecular and Enzymatic Catalysts on Graphene for Biomimetic Generation of Antithrombotic Species. *Nat. Commun.* **2014**, DOI: 10.1038/ncomms4200.
(44) Bitner, B. R.; Marcano, D. C.; Berlin, J. M.; Fabian, R. H.; Cherian, L.; Culver, J. C.; Dickinson, M. E.; Robertson, C. S.; Pautler, R. G.; Kent, T. A.; Tour, J. M. Antioxidant Carbon Particles Improve Cerebrovascular Dysfunction Following Traumatic Brain Injury. *ACS Nano* **2012**, *6*, 8007−8014.
(45) Tian, L.; Anilkumar, P.; Cao, L.; Kong, C. Y.; Meziani, M. J.; Qian, H.; Veca, L. M.; Thorne, T. J.; Tackett, K. N.; Edwards, T.; Sun, Y.-P. Graphene Oxides Dispersing and Hosting Graphene Sheets for Unique Nanocomposite Materials. *ACS Nano* **2011**, *5*, 3052−3058.
(46) Gao, W.; Wu, G.; Janicke, M. T.; Cullen, D. A.; Mukundan, R.; Baldwin, J. K.; Brosha, E. L.; Galande, C.; Ajayan, P. M.; More, K. L.; Dattelbaum, A. M.; Zelenay, P. Ozonated Graphene Oxide Film as a Proton-Exchange Membrane. *Angew. Chem., Int. Ed.* **2014**, *53*, 3588−3593.
(47) Ha, H.; Shanmuganathan, K.; Ellison, C. J. Mechanically Stable Thermally Crosslinked Poly(acrylic acid)/Reduced Graphene Oxide Aerogels. *ACS Appl. Mater. Interfaces* **2015**, *7*, 6220−6229.
(48) Alonso-Cristobal, P.; Vilela, P.; El-Sagheer, A.; Lopez-Cabarcos, E.; Brown, T.; Muskens, O. L.; Rubio-Retama, J.; Kanaras, A. G. Highly Sensitive DNA Sensor Based on Upconversion Nanoparticles and Graphene Oxide. *ACS Appl. Mater. Interfaces* **2015**, *7*, 6220−6229.
(49) Liu, Z.; Robinson, J. T.; Sun, X.; Dai, H. PEGylated Nanographene Oxide for Delivery of Water-Insoluble Cancer Drugs. *J. Am. Chem. Soc.* **2008**, *130*, 10876−10877.
(50) Cho, Y.; Kim, H.; Choi, Y. A Graphene Oxide-Photosensitizer Complex as an Enzyme-Activatable Theranostic Agent. *Chem. Commun.* **2013**, *49*, 1202−1204.
(51) Zhou, L.; Jiang, H. J.; Wei, S. H.; Ge, X. F.; Zhou, J. H.; Shen, J. High-Efficiency Loading of Hypocrellin B on Graphene Oxide for Photodynamic Therapy. *Carbon* **2012**, *50*, 5594−5604.
(52) Li, F.; Park, S.-J.; Ling, D.; Park, W.; Han, J. Y.; Na, K.; Char, K. Hyaluronic Acid-Conjugated Graphene Oxide/Photosensitizer Nanohybrids for Cancer Targeted Photodynamic Therapy. *J. Mater. Chem. B* **2013**, *1*, 1678−1686.
(53) Tian, B.; Wang, C.; Zhang, S.; Feng, L.; Liu, Z. Photothermally Enhanced Photodynamic Therapy Delivered by Nano-Graphene Oxide. *ACS Nano* **2011**, *5*, 7000−7009.
(54) Moore, M. Do Nanoparticles Present Ecotoxicological Risks for the Health of the Aquatic Environment? *Environ. Int.* **2006**, *32*, 967−976.
(55) Maxfield, F. R.; McGraw, T. E. Endocytic Recycling. *Nat. Rev. Mol. Cell Biol.* **2004**, *5*, 121−132.
(56) Xu, J.; Zeng, F.; Wu, H.; Hu, C.; Wu, S. Enhanced Photodynamic Efficiency Achieved via a Dual-Targeted Strategy Based on Photosensitizer/Micelle Structure. *Biomacromolecules* **2014**, *15*, 4249−4259.
(57) Fan, J.; Zeng, F.; Wu, S.; Wang, X. Polymer Micelle with pH-Triggered Hydrophobic−Hydrophilic Transition and De-Cross-Linking Process in the Core and Its Application for Targeted Anticancer Drug Delivery. *Biomacromolecules* **2012**, *13*, 4126−4137.
(58) Zhang, L.; Xia, J.; Zhao, Q.; Liu, L.; Zhang, Z. Functional Graphene Oxide as a Nanocarrier for Controlled Loading and Targeted Delivery of Mixed Anticancer Drugs. *Small* **2010**, *6*, 537−544.
(59) Torring, T.; Helmig, S.; Ogilby, P. R.; Gothelf, K. V. Singlet Oxygen in DNA Nanotechnology. *Acc. Chem. Res.* **2014**, *47*, 1799−1806.
(60) Cho, Y.; Choi, Y. Graphene Oxide/Photosensitizer Conjugate as a Redox-Responsive Theranostic. *Chem. Commun.* **2012**, *48*, 9912−9914.
(61) Qian, H. S.; Guo, H. C.; Ho, P. C. L.; Mahendran, R.; Zhang, Y. Mesoporous-Silica-Coated Up-Conversion Fluorescent Nanoparticles for Photodynamic Therapy. *Small* **2009**, *5*, 2285−2290.
(62) Ly, J.; Grubb, D.; Lawen, A. The Mitochondrial Membrane Potential ($\Delta\psi$m) in Apoptosis; An Update. *Apoptosis* **2003**, *8*, 115−128.
(63) Larsen, A. K.; Malinska, D.; Koszela-Piotrowska, I.; Parhamifar, L.; Hunter, A. C.; Moghimi, S. M. Polyethylenimine-Mediated Impairment of Mitochondrial Membrane Potential, Respiration and Membrane Integrity: Implications for Nucleic Acid Delivery and Gene Therapy. *Mitochondrion* **2012**, *12*, 162−168.

DOI: 10.1021/acsami.5b02297
ACS Appl. Mater. Interfaces 2015, 7, 9287−9296